

20.8% Slot-Die Coated MAPbI₃ Perovskite Solar Cells by Optimal DMSO-Content and Age of 2-ME Based Precursor Inks

Jinzhao Li, Janardan Dagar, Oleksandra Shargaieva, Marion A. Flatken, Hans Köbler, Markus Fenske, Christof Schultz, Bert Stegemann, Justus Just, Daniel M. Többens, Antonio Abate, Rahim Munir, and Eva Unger*

Solar cells incorporating metal-halide perovskite (MHP) semiconductors are continuing to break efficiency records for solution-processed solar cell devices. Scaling MHP-based devices to larger area prototypes requires the development and optimization of scalable process technology and ink formulations that enable reproducible coating results. It is demonstrated that the power conversion efficiency (PCE) of small-area methylammonium lead iodide (MAPbI₃) devices, slot-die coated from a 2-methoxy-ethanol (2-ME) based ink with dimethyl-sulfoxide (DMSO) used as an additive depends on the amount of DMSO and age of the ink formulation. When adding 12 mol% of DMSO, small-area devices of high performance (20.8%) are achieved. The effect of DMSO content and age on the thin film morphology and device performance through in situ X-ray diffraction and small-angle X-ray scattering experiments is rationalized. Adding a limited amount of DMSO prevents the formation of a crystalline intermediate phase related to MAPbI₃ and 2-ME (MAPbI₃-2-ME) and induces the formation of the MAPbI₃ perovskite phase. Higher DMSO content leads to the precipitation of the (DMSO)₂MA₂Pb₃I₈ intermediate phase that negatively affects the thin-film morphology. These results demonstrate that rational insights into the ink composition and process control are critical to enable reproducible large-scale manufacturing of MHP-based devices for commercial applications.


1. Introduction

Metal-halide perovskite (MHP) semiconductors are of interest for various optoelectronic devices: photovoltaics (PV),^[1–4] light-emitting diodes (LED),^[5] lasers,^[6] and photodetectors.^[7] With 25% power conversion efficiency (PCE),^[8] MHP solar cell devices are the best solution-processed solar cell devices to date.^[2] Having reached performance on par with other thin-film devices in laboratory-scale test devices, scaling MHP-based solar cells to a larger area is one of the technologically most important steps.

A variety of scalable fabrication techniques such as blade-coating,^[9] vapor-assisted deposition,^[10] inkjet printing,^[11] and slot-die coating (SDC)^[12] have been successfully utilized for the deposition of MHP materials. Notably, SDC is considered as one of the most promising deposition techniques in the fabrication of functional coating and solution-processed optoelectronics as uniform and compact thin-films can be processed on both rigid and flexible

J. Li, Dr. J. Dagar, Dr. O. Shargaieva, M. Fenske, Dr. R. Munir, Dr. E. Unger
Helmholtz-Zentrum Berlin für Materialien und Energie GmbH
HySPRINT Innovation Lab
Young Investigator Group Hybrid Materials Formation and Scaling
Kekuléstr. 5 12489, Berlin Germany
E-mail: eva.unger@helmholtz-berlin.de

M. A. Flatken, H. Köbler, Dr. A. Abate
Helmholtz-Zentrum Berlin für Materialien und Energie GmbH
HySPRINT Innovation Lab
Young Investigation Group Active Materials and Interfaces for Stable
Perovskite Solar Cells
Kekuléstr. 5 12489, Berlin Germany

 The ORCID identification number(s) for the author(s) of this article can be found under <https://doi.org/10.1002/aenm.202003460>.

© 2021 The Authors. Advanced Energy Materials published by Wiley-VCH GmbH. This is an open access article under the terms of the Creative Commons Attribution License, which permits use, distribution and reproduction in any medium, provided the original work is properly cited.

C. Schultz, Prof. B. Stegemann
University of Applied Sciences - HTW Berlin
Wilhelmshofstr. 75a D-12459, Berlin Germany

Dr. J. Just
MAX IV Laboratory
Lund University
P.O. Box 118, Lund SE-221 00, Sweden

Dr. D. M. Többens
Helmholtz-Zentrum Berlin für Materialien und Energie GmbH
Department Structure and Dynamics of Energy Materials
Albert-Einstein-Str. 15 12489, Berlin Germany

Dr. R. Munir
Department of Chemistry
University of Calgary
Calgary T2N 1N4, Canada

Dr. E. Unger
Chemical Physics and Nano Lund
Lund University
P.O. Box 124, Lund 22100, Sweden

DOI: 10.1002/aenm.202003460

substrates.^[13] When coating crystalline (or crystallizing) materials such as MHP, the quality of the thin-film is determined by the coating process. Fabricating high-quality thin-films requires exact control over the process window and removal of solvents at a defined period of time to induce oversaturation and crystallization in a controlled manner. Solvent removal can be facilitated by thermal annealing,^[14] vacuum,^[12] gas quenching^[15] or the deposition of an anti-solvent, which for larger area samples is often accomplished by dipping into a bath.^[16]

Currently, the PCE obtained for slot-die coated devices is lower than record device PCEs achieved by spin-coating.^[17] This is due to the fact that there has been considerably less optimization work on SDC for MHP deposition and record-performance spin-coated devices rely on rapid solvent removal and induction of crystallization by deposition of an anti-solvent. One of the most important aspects to optimize slot-die coating for MHP deposition is to develop reproducible coating processes where the MHP crystallization is selectively induced during the coating process.^[18] Process optimization and design of stable precursor inks that enable the deposition of high quality MHP layers that yield higher PCE in solar cell devices.

In this work, we successfully slot-die coated methylammonium lead iodide (MAPbI₃) thin films from a low boiling point and highly soluble 2-methoxy-ethanol (2-ME) ink as previously introduced by Hendriks et al. for spin-coating.^[19] Deng et al. adopted this ink to realize blade-coated PSCs^[9] introducing the strongly coordinating solvent dimethyl sulfoxide (DMSO) to improve the quality of coated perovskite thin films. We explain, why also record-performance slot-die coated PSCs can be manufactured following this procedure and provide a detailed investigation on how the exact amount of DMSO and age of the precursor ink affects thin-film morphology as well as device performance. Record performance devices of up to 20.8% power conversion efficiency were achieved when adding ≈12 mol% of DMSO in the precursor solution. Using in situ grazing incidence X-ray scattering and small-angle X-ray scattering experiments, we can prove that adding a small amount of DMSO leads to the suppression of colloidal structures in solution and crystalline intermediate phase related to MAPbI₃ and 2-ME (here referred to as MAPbI₃-2-ME). Instead, MAPbI₃ seed crystals and a limited amount of the (DMSO)₂MA₂Pb₃I₈ intermediate phase are formed having a beneficial effect on thin-film formation. A larger amount of DMSO and with proceeding age of the precursor solution, the precipitation of the crystalline (DMSO)₂MA₂Pb₃I₈ solvate phase^[20] becomes detrimental to the perovskite thin film morphology. We highlight that both the exact amount of DMSO as well as the age of the precursor solution critically affect the coating results and device performance. This insight enabled the development of stable and reproducible coating procedure for large scale manufacturing of perovskite solar cell devices. First attempts to make mini-modules based on our optimized ink recipe and process parameters to achieve an efficiency of close to 15% on a very small module of 2.2 cm² active area with three interconnected subcells.

2. Results and Discussion

Detailed experimental details on sample preparation and characterization can be found in the Supporting Information. As

metal-halide perovskites (MHPs) tends to crystallize during deposition, the removal of solvents at a defined point in time determines the thin-film quality. This provides some but limited control over the process window and the exact composition of the ink has a significant influence on the quality of the MHP semiconductor. In the process discussed here, the induction of thin-film crystallization was achieved by N₂ gas quenching through an air knife at around 20 cm distance relative to the slot-die as illustrated in **Figure 1** or with an N₂ gun during spin-coating (Section S2.3, Supporting Information).

We here investigated the combination of the addition of a strongly coordinating solvent dimethyl sulfoxide (DMSO) to a methylammonium lead iodide (MAPbI₃) precursor solution in 2-methoxy ethanol (2-ME). 2-ME is a low boiling point ($T_b = 124$ °C) and high vapor pressure (≈0.8 kPa at 20 °C) solvent with a maximum solubility of MAPbI₃ around 2.4 m.^[19] During coating, the ink is dispensed from the slot-die head onto the substrates, as sketched in **Figure 1a**. We observe that MHP films coated from pure 2-ME solutions were discontinuous and porous as shown in the cross-sectional SEM image in **Figure 1b**. The pinhole density of these samples was about 7% (**Figure S1**, Supporting Information). We attribute this to a rapid and disordered crystallization process when 2-ME spontaneously evaporates during coating and air knife gas quenching.

The addition of small amounts of the strongly coordinating solvent DMSO led to dramatic changes of the resulting thin-film morphology. In **Figure 1b**, the cross-sectional images of samples coated from inks with various amounts of DMSO, ranging from 11.77 mol% to 58.88 mol%, are compared to samples coated from precursor solution not containing any DMSO. The addition of 11.77 mol% DMSO into 1M 2-ME ink leads to a denser thin-film without pinholes and large columnar crystallites. For higher DMSO contents thin-films are still dense and pinhole-free but the crystallite size becomes smaller as shown in **Figure S1** (Supporting Information).

We carried out photoluminescence (PL) measurements on those corresponding thin films, as shown in **Figure S2** (Supporting Information). The PL intensity of perovskite coated with 2-ME DMSO inks is similar in intensity but there is a slight blue-shift of the PL peak maximum, which could be indicative of slight differences in the average grain size. Samples fabricated based on the pure 2-ME MAPbI₃ ink, exhibit a lower PL intensity indicating lower sample quality and more nonradiative recombination.

Precursor inks with added DMSO exhibited a yellow precipitate increasing with time and DMSO content when stored at room temperature as shown in **Figure 1d**. The 2-ME precursor ink without DMSO and the 2-ME based ink comprising 11.8 mol% of added DMSO do not exhibit this precipitate. This suggests a chemical interaction between the DMSO and perovskite precursors. As previously reported,^[9] without the addition of MAI, PbI₂ has a limited solubility in 2-ME. A strongly coordinating solvent like DMSO can be expected to increase the solubility of the precursor salts in 2-ME. DMSO is known to interact strongly with lead-iodide complexes in solution and form a crystalline intermediate phase ((DMSO)₂MA₂Pb₃I₈) upon drying.^[21] The precipitate formed in 2-ME solutions was identified as (DMSO)₂MA₂Pb₃I₈ by X-ray diffraction^[21] (**Figure S3**, Supporting Information) showing that the DMSO solvate phase has indeed a limited solubility in 2-ME.

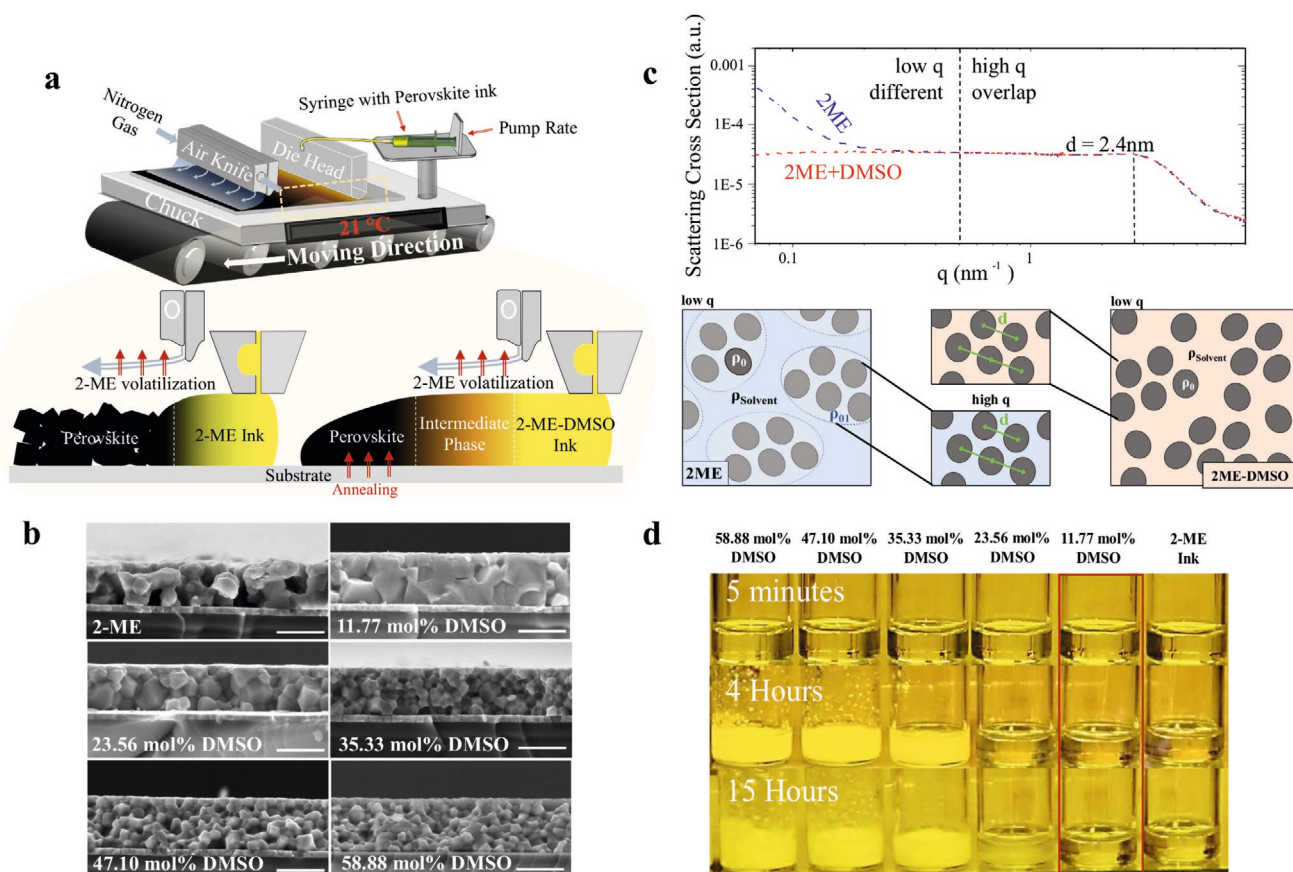


Figure 1. Schematic of slot die coater setup. a) Coating from 2-ME and 2-ME-DMSO inks. b) SEM cross-section images depicting corresponding conditions (scale bar is 800 nm). c) SAXS curves of two backgrounds subtracted scattering curves of MAPbI₃ in 2-ME (blue) compared to MAPI in 2-ME with 11.77 mol% DMSO (red), both solutions are in the same concentration. The schematic representation of contrast situations that can be interpreted from the SAXS curves. The information at high q values matches. The contrast situation changes for the low q -region, which therefore results in two different model approaches for MAPbI₃ in 2-ME (light blue) and MAPbI₃ in 2-ME with 11.77 mol% DMSO (light red). d) Images of 2-ME DMSO inks (in duration of 1 to 15 h) store inside the glovebox (with O₂ and H₂O level less than 1 ppm).

To investigate the effect of the DMSO addition on the ink properties further, we carried out small angle X-ray scattering (SAXS), UV-Vis absorption measurements and X-ray absorption fine structure (EXAFS) measurements further discussed in the Supporting Information. In Figure 1c, the SAXS measurements on the 2-ME and 2-ME-DMSO perovskite inks are compared showing that there is a clear difference in their colloidal properties.^[22–24] It is clearly visible that both inks have the same features in the higher q -values. The observed structure factor maximum ($q = 2.6$ nm⁻¹), which emerges from the interaction of particles, is located at the same position. This indicates that the mean spacing d between the centers of mass of the colloidal particles ($d = 2.4$ nm) is the similar and the nearest-range order between lead-halide complexes in solution comparable. We also carried out extended X-ray absorption fine structure (EXAFS) measurements and found that the local surrounding of lead complexes is similar for all inks (Figure S4, Supporting Information). In the SAXS measurements the slope of the scattering curve deviates at lower q -values, which indicates a substantial difference in the electron density of the particle with respect to their surrounding media (solvent), ($\rho_0 \cdot \rho_{\text{solvent}}$).^[25] The additional scattering contrast at low q values for the 2-ME ink indicates

an interaction between solution complexes forming larger colloidal structures. This preassociation of larger agglomerates is likely the reason for the formation of very porous thin-films deposited from pure 2-ME inks. The ink with additional DMSO has more evenly dispersed colloids which is favorable for prevent the formation of MAPbI₃-2-ME intermediate phase and the formation of denser thin-films. From UV-Vis absorption measurements, precursor solutions appeared to have quite similar absorption features for freshly made samples (Figure S5, Supporting Information). Inks with increasing DMSO content exhibit a reduced and broadened signature probably do to the precipitation of (DMSO)₂MA₂Pb₃I₈.

In situ grazing-incidence wide-angle X-ray scattering (GIWAXS) experiments were utilized both to characterize prepared thin films by ex situ measurements (Figures S8 and S9, Supporting Information) as well as to investigate the drying kinetics for inks with varying DMSO content (Figure 2, Figures S6 and S7, Supporting Information). As shown in Figure 2a, the sample deposited from 2-ME ink initially (start to 0.5 min) exhibits broad features at low diffraction angles indicating the presence of a crystalline sol-gel intermediate state consistent with the SAXS results. In the 2D representation of

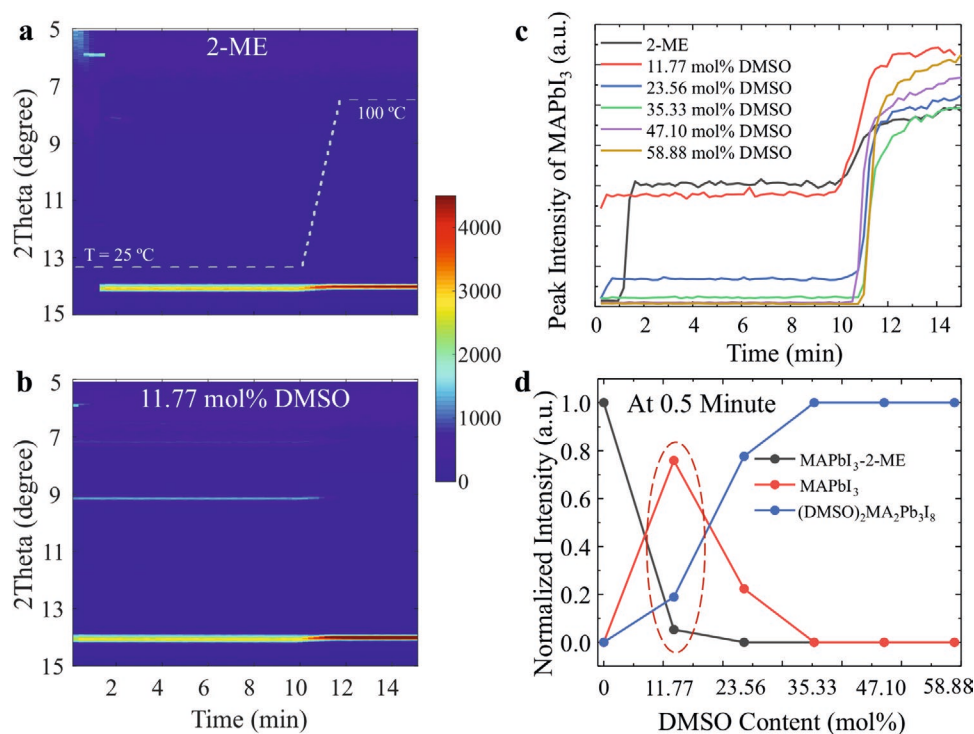


Figure 2. In situ GIWAXS measurements. a,b) 2D plots of time resolved in situ grazing incidence wide-angle X-ray scattering (GIWAXS) of a) 2-ME ink and b) 11.77 mol% 2-ME-DMSO ink (Temperature keep at 25 °C from 0 to 10 min, then accelerating to 100 °C with ramping of 45 °C min⁻¹). c) Normalized peak intensity of MAPbI₃ versus of time. d) MAPbI₃-2-ME, MAPbI₃ and (DMSO)₂MA₂Pb₃I₈ as function of DMSO content at 0.5 minute of in situ GIWAXS pattern.

the evolution of diffraction patterns during drying, diffraction peaks at 2θ angles of 5.92° and 11.86° are visible until about 1 min into the process. We attribute these to a crystalline solvate intermediate phase of MAPbI₃ with 2-ME that has not been previously reported. Upon drying, an intermediate peak at 2θ angles of 8.15° , appearing after 1.4 min and disappearing after 3 min, indicates the formation of another intermediate phase. This phase may be comparable to the (MA)₈(Sol)_xPb₁₈I₄₄ intermediate phase reported by Lei et al. which exhibits diffraction features in the same range.^[26] We conclude that fast evaporation of 2-ME results in the rapid transformation of this intermediate phase into the MHP phase after only 1 min at 25 °C. This can be observed as an evolution of the diffraction peak at 14.08° that correlates with the (110/002) peaks of the room temperature tetragonal MAPbI₃ phase.^[27] It can be noted that the MHP peak intensity is relatively high, indicating rapid crystallization of the MHP as 2-ME solvent starts evaporating.

When adding 11.77 mol% of DMSO into 1 M 2-ME ink as shown in Figure 2b, a reduced diffraction peak at 5.92° suggest the initial coexistence of the intermediate phases of MAPbI₃-2-ME and the DMSO solvate phase with known diffraction peaks at 6.55° , 7.2° , 9.17° attributed to the formation of the (DMSO)₂MA₂Pb₃I₈ phase during the first 0.5 minute of the drying process.^[21] There is no peak at 8.15° visible in this case suggesting that the formation of this second intermediate phase is suppressed. Instead, a diffraction pattern is consistent with the formation of crystalline MAPbI₃ is visible from the start as shown in Figure 2c,d. We interpret these findings that the DMSO additive avoids the formation of the 2-ME solvate phase

and triggers the formation of MAPbI₃ as well as DMSO solvate phase. These results indicate the formation of MAPbI₃ seed crystals upon addition of DMSO, which favorably affects thin film formation. We hypothesize, that the much higher binding constant of DMSO to lead-halide complexes in solution disrupts the formation of the 2-ME and other solvate intermediate phases to promote the formation of crystalline MAPbI₃. Simultaneously, (DMSO)₂MA₂Pb₃I₈ is also formed, which, at small concentrations, may prove beneficial to thin film formation as it may increase the processing window. That the formation of the (DMSO)₂MA₂Pb₃I₈ intermediate phase is detrimental at higher concentration becomes apparent when increasing to the amount of added DMSO to over 11.77 mol% (Figure 2d), which leads to a disappearance of any MAPbI₃-2-ME intermediate but also the MAPbI₃ phase in favor of (DMSO)₂MA₂Pb₃I₈. The formation of the DMSO solvate phase occurs already in solution apparent by the formation of the yellowish precipitate in precursor solutions shown in Figure 1d. In this case, MAPbI₃ has to and increasing extent be formed by decomposition of the DMSO intermediate phase. This negatively affects the thin-film morphology as shown in the SEM cross section images in Figure 1b. To compare ink properties, ex situ GIWAXS was employed to detect crystallinity and orientation of MHP semiconductors. We did not observe a change in orientation, indicating the crystal growth orientation was not affected by the addition of DMSO (Figure S8, Supporting Information). However, the 2ME-DMSO samples exhibit an increased intensity of the diffraction peaks associated with the perovskite crystal phase. We conclude that the addition of DMSO improves the

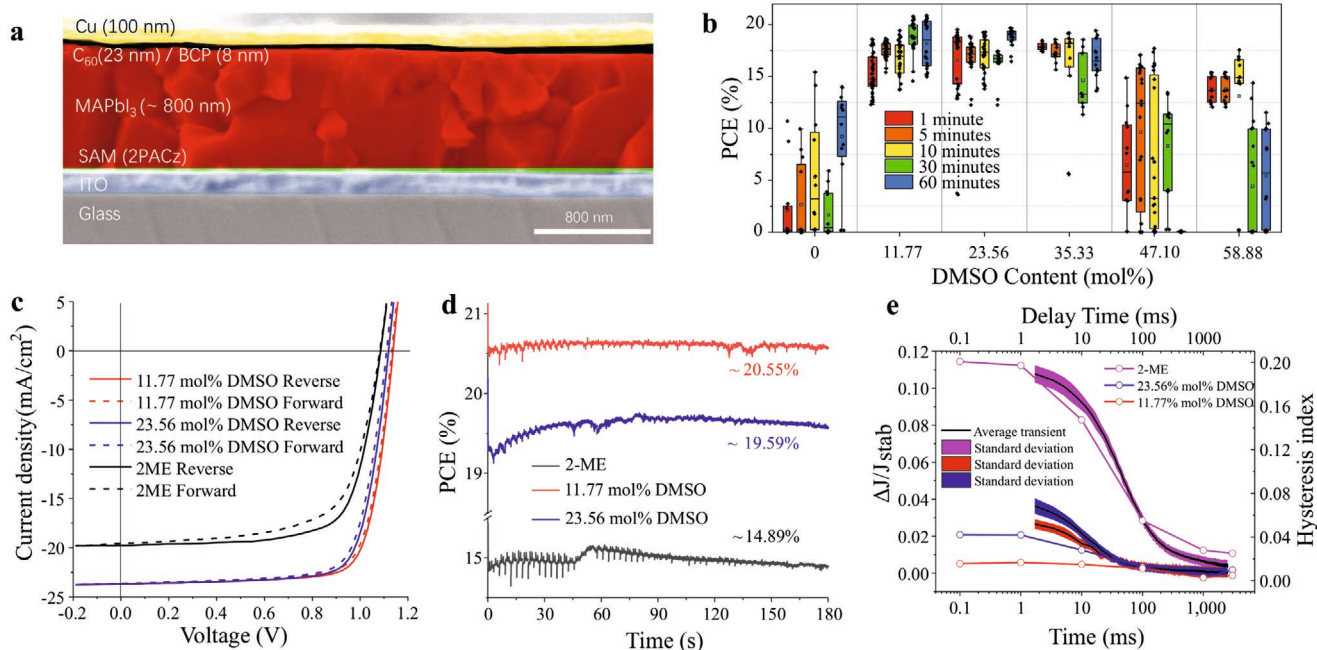


Figure 3. Devices performance and parameters. a) configuration and cross-sectional images of device made from 11.77 mol% 2-ME-DMSO ink. b) The performance distribution of more than 60 solar cell devices made by 2-ME and 2-ME-DMSO inks was summarized versus storage time. c) The current density–voltage (J – V) scanning (active area is 0.16 cm^2) and d) the stabilized output of the corresponding devices. e) The differential transient response of devices upon voltage perturbation at MPP $\Delta J/J_{\text{stab}}$, and hysteresis index (HI) derived from reverse and forward the J – V measurements at different delay times of devices fabricated from 2-ME reference and 11.77 mol% as well as 23.56 mol% DMSO containing 2-ME inks.

crystallinity of the thin-film sample (Figure S9, Supporting Information).

To study the stability of precursor inks, a series of solar cell devices were prepared from precursor inks with various amounts of DMSO (11.77 mol%–58.88 mol%) and time elapsed since preparation of the ink 1, 5, 10, 30, and 60 min in comparison to the reference ink. Figure 3a show the device configuration is glass | ITO (150 nm) | 2PACz | MAPbI₃ (\approx 800 nm) | C₆₀ (23 nm) | BCP (8 nm) | Cu (100 nm) where 2PACz is a self-assembled monolayer (SAM) of ([2-(9H-carbazol-9-yl)ethyl] phosphonic acid)). The results shown in Figure 3b clearly illustrate the dependency of the power conversion efficiency, PCE, of solar cells on the DMSO content and age of the precursor ink. The devices made from the 2-ME reference ink exhibit fairly low and irreproducible performance metrics. For an increasing content of DMSO in the 2-ME precursor inks, the average performance and reproducibility initially increases for intermediate DMSO concentrations of about 12 and 24 mol% but then clearly decreases for higher DMSO content and also with increasing ink age. All the device performance metrics of open circuit voltage, V_{OC} , short-circuit current density, J_{SC} , and fill factor, FF, are negatively affected for the ink without the DMSO additive and with an increasing DMSO content >24 mol% (Figure S10, Supporting Information). We attribute this to the bad sample morphology for samples prepared from pure 2-ME inks due to unfavorable drying kinetics as well as the detrimental effect of thin-film morphology upon formation of the (DMSO)₂(MA)₂Pb₃I₈ precipitate in inks of higher DMSO content. Precipitation of a solid phase is likely detrimental for the rheological properties and flow of ink within

the narrow tubing and ink reservoir of the slot-die coater and will probably influence the pump rate and solution feed during the coating process. This leads to random and unreproducible deposition conditions along with the likely deposition of the (DMSO)₂(MA)₂Pb₃I₈ precipitate, which negatively affects the thin-film morphology. To investigate the influence of precipitation on the film nucleation, 23.56 mol% 2ME-DMSO ink was centrifuged at 6 000 rpm for 45 min with this ink without centrifuged were compared, which resulted in similar devices performance (Figure S11, Supporting Information) and indicates that the precipitate affects the coating process negatively.

Optimal contents of DMSO are crucial to stabilize MHP inks. The 11.77 mol% DMSO ink exhibits better long-term stability than the others investigated herein. Even after storing this ink for 18 d, solar cells with a performance of 19.50% were manufactured as shown in Figure S12 (Supporting Information). After storage for 18 d, the 23.56 mol% DMSO content ink exhibited precipitation and could not be used to produce good quality coatings at all. Figure 3b shows the statistical performance of devices fabricated by different amounts of 2-ME-DMSO inks as function of time and statistical plot of more than 60 subdevices, as shown in Figure S12 (Supporting Information), which suggest 11.77 mol% and 23.56 mol% 2-ME-DMSO devices has small spread. The less amount of DMSO ink has stable and reproducible results. Table 1 summarizes the devices prepared from the 11.77 mol% and 23.56 mol% 2-ME-DMSO precursor inks yielded a maximum PCE of 20.83%, 20.25% with average efficiencies of 17.18%, 17.21% compared to 15.42% (4.2%) for the pure 2-ME reference devices. These PCEs are among the highest values reported for slot-die coated PSCs

Table 1. Summaries of photovoltaic parameters obtained from corresponding J - V curves.

	J_{sc} [mA cm ⁻²]	$J_{sc,mean}^a)$ [mA cm ⁻²]	V_{oc} [V]	$V_{oc,mean}^a)$ [V]	Fill factor[%]	Fill factor _{mean} ^{a)} [%]	PCE [%]	PCE _{mpp} [%]	PCE _{mean} ^{a)} [%]
2-ME reverse	19.778	14.412 ± 4.97	1.085	0.571 ± 0.46	71.870	0.408 ± 0.19	15.424	14.89	4.2 ± 4.95
2-ME forward	19.565		1.082		66.860		14.155		
11.77 mol% 2-ME-DMSO reverse	23.673	22.024 ± 1.03	1.138	1.088 ± 0.03	77.322	0.715 ± 0.05	20.831	20.55	17.18 ± 2.01
11.77 mol% 2-ME-DMSO forward	23.633		1.132		76.426		20.459		
23.56 mol% 2-ME-DMSO reverse	23.686	21.551 ± 0.825	1.119	1.090 ± 0.05	76.415	0.729 ± 0.05	20.256	19.59	17.21 ± 2.12
23.56 mol% 2-ME-DMSO forward	23.645		1.111		75.343		19.793		

^{a)}The values in the parentheses are average from 60 independent sub-cells with standard deviation.

(Table S1, Supporting Information). The steady-state results of corresponding devices, showing PCE of 20.55%, 19.59% and 14.89% upon 180 s maximum power point (MPP) tracking as shown in Figure 3d.

To validate that slot-die coating can yield devices with performance comparable to the commonly used spin-coating technique for the deposition of the perovskite layer, we fabricated spin-coated solar cell devices for the optimized ink with 11.77 mol% of DMSO. We also compared results for depositing the 2PACz self-assembled monolayer by slot-die coating. The resulting device data is summarized in Figure S13 (Supporting Information). The average efficiencies of devices using slot-die coating compared to spin-coating for the deposition of the 2PACz layer are comparable. Spin-coating the MAPbI₃ ink with 11.77 mol% of DMSO, we employed N₂ gas quenching with an N₂ gun during spin-coating. Devices exhibited decent results with similar average performance as the slot-die coated devices. Our findings suggest that devices with performances comparable or even higher can be obtained when using a scalable solution-based technique such as slot-die coating for the deposition of the MAPbI₃ semiconductor. We predict that slot-die coated devices rivalling or beating spin-coated small area record devices will be achieved in the very near future with additional ink and process optimization.

The stability assessment of the champion devices was performed via MPP tracking under continuous 1 sun illumination for 11 h. We observed a stabilized device efficiency of 19.16% before tracking and 19.24% after tracking for this particular device suggesting a negligible loss in efficiency as shown in Figure S14 (Supporting Information). Furthermore, the long-term continuous MPP tracking of 11.77 mol% DMSO devices is shown in Figure S15 (Supporting Information). After 500 h tracking, the device retained over 90% of its initially performance with mainly loss in the fill factor. We compared the device performance with and without shadow mask and found around 3% discrepancy in the J_{sc} (Figure S16 and Table S2, Supporting Information). Comparing the integrated external quantum efficiency, EQE, spectra with respect to AM1.5G results in J_{sc} values comparable to the ones determined by J - V measurements (Figure S17, Supporting Information) with a discrepancy <4%. Additionally, the bandgaps are around 1.58–1.59 eV determining by the peak position of the derivative of the EQE spectrum. The 2-ME-DMSO devices exhibit lower leakage current (J_0) in the dark J - V curves (Figure S18, Supporting Information) compared to the 2-ME device, which we

interpret to be a result of the superior MHP layer morphology and coverage. The 11.77 mol% 2-ME-DMSO device shows an improved rectification leading to the better performance in the reverse bias condition of the MHP based solar cell.^[28]

Transient analysis during maximum power point tracking (TrAMPPT) was used to investigate the devices transient response upon voltage perturbation,^[29,30] further discussed in the Supporting Information. The comparison of the current transients with respect to the steady-state current density, $\frac{\Delta J(t)}{J_{ss}}$

and the hysteresis index, $HI = \frac{PCE_{rev} - PCE_{fwd}}{PCE_{rev}}$, as a function of

the delay time derived from J - V measurements (Figures S19, S20 and S21, Supporting Information) is compared in Figure 3e for devices made from the pure 2-ME-based ink as well as from inks with 11.77 mol% and 23.56 mol% of added DMSO. The devices prepared from precursor solutions with DMSO exhibit a dramatically reduced amplitude of the $\frac{\Delta J(t)}{J_{ss}}$ as well as HI for

fast scan rates corresponding to short delay times. The device fabricated from the pure 2-ME precursor ink exhibits a more pronounced amplitude of the transient current response for fast J - V scan rates compared to the devices fabricated from inks containing small amounts of DMSO where this transient current response is fairly suppressed. This directly corresponds to a reduction of the hysteresis observed at fast scan rates, which indicate capacitive charge carrier accumulation effects or a sluggish charge carrier extraction for devices with inferior perovskite thin-film morphology. We conclude that the smaller grain size and higher degree of disorder and pinholes of samples prepared without the DMSO additive in the precursor solutions gives rise to a lower charge carrier extraction efficiency and hence larger amplitudes in the transient current response upon voltage perturbation.

We carried out first attempts to manufacture slot-die coated minimodules based on optimized ink and process conditions. Details can be found in the Supporting Information. One set of minimodules were fabricated on substrates of similar size as our small-area test devices (inch² ≈ 2.5 × 2.5 cm²) and also on 5 × 5 cm² substrates. Series-interconnection of subcells in the minimodule was realized by P1–P2–P3 laser-interconnection schemes optimized previously, sketched in Figure S22 (Supporting Information).^[31] As laser-patterning step had to be carried out in ambient conditions, we replaced the BCP with an ALD-deposited layer of 20 nm SnO₂ in our devices, as detailed

in the Supporting Information. For the $2.5 \times 2.5 \text{ cm}^2$ substrates, three subcells were implemented with a total active device area of 2.2 cm^2 , as shown in the Figure S23 (Supporting Information). The PCE statistics of 15 minimodules showed the average value of 9.3% and champion efficiency of 14.6% with negligible hysteresis. Figure S24 (Supporting Information) show $5 \times 5 \text{ cm}^2$ substrates, modules comprised eight series-interconnected sub-cells. The average device performance was only 1.8% with the highest performance of 3.8% achieved due to obvious losses in both open-circuit voltage and fill factor.

While the first results on minimodules are encouraging, more work is required to identify performance loss channels in these modules. Our work highlights the importance of optimizing inks for scaled metal-halide perovskite layer deposition in combination with the optimization of process conditions. We will carry out more work on optimizing the device layer stack and processes to make larger are minimodules in the future.

3. Conclusions

We were able to achieve highly PCEs of slot-die coated perovskite solar cells reproducibly when just the right amount of DMSO is added to 2-ME based precursor solutions. For an amount of about 12 mol% DMSO, a stable ink with a beneficial coating process window can be obtained enabling the deposition of high-quality MHP thin-films and high-performance solar cell devices. From in-situ X-ray diffraction experiments we have discovered the existence of a solvent intermediate phase involving 2-ME and MAPbI_3 which rapidly converts to MAPbI_3 upon drying. The addition of DMSO leads to the suppression of this intermediate phase and formation of MAPbI_3 seed crystals as well as some $(\text{DMSO})_2\text{MA}_2\text{Pb}_3\text{I}_8$ intermediate phase, which favorably affects the formation process of MAPbI_3 during slot-die coating. This leads to MAPbI_3 thin-films with improved morphology. For a higher DMSO content the suppression of MAPbI_3 formation in favor of $(\text{DMSO})_2\text{MA}_2\text{Pb}_3\text{I}_8$ reduces thin-film layer quality and reproducibility as the crystalline DMSO-solvate phase precipitate negative affects thin-film formation and morphology. From inks with optimal DMSO content, slot-die coated p-i-n solar cell device with efficiency of 20.83% (stabilized output at 20.55%) were demonstrated. This work provides important insight into the interplay of strongly and weakly coordinating solvent as well as crystalline intermediate phases in the formation of MHP thin films. Control over exact processing conditions and formation pathways is key to develop stable and reproducible scalable coating procedures, which is crucial for the commercial fabrication of MHP semiconductor devices.

Supporting Information

Supporting Information is available from the Wiley Online Library or from the author.

Acknowledgements

J.Z.L. and J.D. contributed equally to this work. J.Z.L. acknowledges funding from the Chinese Scholarship Council (CSC, grant No.

CSC201908120116) and HyPerCells joint Graduate School. E.U. and her team acknowledge funding from the German Ministry of Education and Research (BMBF) for the Young Investigator Group Hybrid Materials Formation and Scaling (HyPerFORME) within the program "NanoMatFutur" (grant no. 03XP0091) and the SNaPSHoTs project (grant no. 01IO1806). E.U. and J.J. acknowledge funding from the Swedish Foundation for Strategic Research (SSF, Project ITM17-0276). Lab infrastructure in the Helmholtz Innovation Lab was supported by the Helmholtz Energy Materials Foundry (HEMF) and the PEROSEED (ZT-0024) project, as well as the support of the. Allocation of synchrotron radiation beamtime at PTB and KMC-2, BESSY II, HZB, Germany and the Balder beamline at MAXIV, Sweden are gratefully acknowledged. J.Z.L. acknowledged Dr. Kajsa Sigfridsson Clauss and Hampus Näsström for their kindly assistance during beamtime measurements at the Balder beamline at MAXIV, Sweden. J.Z.L. thanks Ke Xu, Dr. Fengjiu Yang and Dr. Steve Albrecht (Young Investigator Group Perovskite Tandem Solar Cells) for support with the atomic layer deposition. All authors acknowledge M. Gabernig, C. Ferber, T. Lußky, H. Heinz and C. Klimm at Helmholtz-Zentrum Berlin (HZB) for technical support. M.A.F. thanks Armin Hoell and the PTB for the ability to use their facilities at BESSY II. Open access funding enabled and organized by Projekt DEAL.

Conflict of Interest

The authors declare no conflict of interest.

Data Availability Statement

Data available on request from the authors.

Keywords

ink age, perovskite solar cells, slot-die coating, SAXS, WAXS

Received: November 2, 2020

Revised: December 27, 2020

Published online: January 25, 2021

- [1] A. Kojima, K. Teshima, Y. Shirai, T. Miyasaka, *J. Am. Chem. Soc.* **2009**, *131*, 6050.
- [2] X. Zheng, Y. Hou, C. Bao, J. Yin, F. Yuan, Z. Huang, K. Song, J. Liu, J. Troughton, N. Gasparini, C. Zhou, Y. Lin, D. J. Xue, B. Chen, A. K. Johnston, N. Wei, M. N. Hedhili, M. Wei, A. Y. Alsalloum, P. Maity, B. Turedi, C. Yang, D. Baran, T. D. Anthopoulos, Y. Han, Z. H. Lu, O. F. Mohammed, F. Gao, E. H. Sargent, O. M. Bakr, *Nat. Energy* **2020**, *5*, 131.
- [3] H. J. Lee, M. M. Teuscher, J. Miyasaka, T. Murakami, T. Snaith, *Science* **2012**, *338*, 643.
- [4] F. Sahlí, J. Werner, B. A. Kamino, M. Bräuninger, R. Monnard, B. Paviet-Salomon, L. Barraud, L. Ding, J. J. Diaz Leon, D. Sacchetto, G. Cattaneo, M. Despeisse, M. Boccard, S. Nicolay, Q. Jeangros, B. Niesen, C. Ballif, *Nat. Mater.* **2018**, *17*, 820.
- [5] M. Liu, Y. Chen, C.-S. Tan, R. Quintero-Bermudez, A. H. Proppe, R. Munir, H. Tan, O. Voznyy, B. Scheffel, G. Walters, A. P. T. Kam, B. Sun, M.-J. Choi, S. Hoogland, A. Amassian, S. O. Kelley, F. P. García de Arquer, E. H. Sargent, *Nature* **2019**, *570*, 96.
- [6] N. Zhang, Y. Fan, K. Wang, Z. Gu, Y. Wang, L. Ge, S. Xiao, Q. Song, *Nat. Commun.* **2019**, *10*, 1770.
- [7] J. Miao, F. Zhang, *J. Mater. Chem. C* **2019**, *7*, 1741.
- [8] Best Research-Cell Efficiency Chart (NREL), <https://www.nrel.gov/pv/cell-efficiency.html> (accessed: August 2020).

- [9] Y. Deng, C. H. Van Brackle, X. Dai, J. Zhao, B. Chen, J. Huang, *Sci. Adv.* **2019**, 5, eaax7537.
- [10] J. Li, H. Cao, X. Wang, H. Zhu, Z. Dong, L. Yang, S. Yin, *ACS Appl. Energy Mater.* **2019**, 2, 2506.
- [11] F. Mathies, E. J. W. List-Kratochvil, E. L. Unger, *Energy Technol.* **2019**, 81, ente.201900991.
- [12] L. Cai, L. Liang, J. Wu, B. Ding, L. Gao, B. Fan, *J. Semicond.* **2017**, 38, 2.
- [13] E. Lim, J. Yao, *IFAC Proc.* **2009**, 7, 405.
- [14] D. Burkitt, J. Searle, D. A. Worsley, T. Watson, *Materials* **2018**, 11, 2106.
- [15] D. Lee, Y. S. Jung, Y. J. Heo, S. Lee, K. Hwang, Y. J. Jeon, J. E. Kim, J. Park, G. Y. Jung, D. Y. Kim, *ACS Appl. Mater. Interfaces* **2018**, 10, 16133.
- [16] J. Whitaker, D. Kim, B. W. Larson, F. Zhang, J. J. Berry, M. F. A. M. van Hest, K. Zhu, *Sustainable Energy Fuels* **2018**, 2, 2442.
- [17] Z. Li, T. R. Klein, D. H. Kim, M. Yang, J. J. Berry, M. F. A. M. Van Hest, K. Zhu, *Nat. Rev. Mater.* **2018**, 3, 18017.
- [18] Y. Wu, A. Islam, X. Yang, C. Qin, J. Liu, K. Zhang, W. Peng, L. Han, *Energy Environ. Sci.* **2014**, 7, 2934.
- [19] K. H. Hendriks, J. J. Van Franeker, B. J. Bruijnaers, J. A. Anta, M. M. Wienk, R. A. J. Janssen, *J. Mater. Chem. A* **2017**, 5, 2346.
- [20] J. W. Lee, H. S. Kim, N. G. Park, *Acc. Chem. Res.* **2016**, 49, 311.
- [21] Y. Rong, Z. Tang, Y. Zhao, X. Zhong, S. Venkatesan, H. Graham, M. Patton, Y. Jing, A. M. Guloy, Y. Yao, *Nanoscale* **2015**, 7, 10595.
- [22] H. Schnablegger, Y. Singh, *The SAXS Guide*, Anton Paar GmbH, Graz, Austria **2013**.
- [23] R. F. Moral, L. G. Bonato, J. C. Germino, W. X. Coelho Oliveira, R. Kamat, J. Xu, C. J. Tassone, S. D. Stranks, M. F. Toney, A. F. Nogueira, *Chem. Mater.* **2019**, 31, 9472.
- [24] M. Krumrey, G. Ulm, *Nucl. Instrum. Methods Phys. Res., Sect. A* **2001**, 467, 1175.
- [25] D. I. Svergun, M. H. J. Koch, P. A. Timmins, R. P. May, *Small Angle X-Ray and Neutron Scattering from Solutions of Biological Macromolecules*, Oxford University Press, Oxford **2013**.
- [26] L. Lei, M. Li, D. M. Grant, S. Yang, Y. Yu, J. A. Watts, D. B. Amabilino, *Chem. Mater.* **2020**, 32, 5958.
- [27] C. Quarti, E. Mosconi, J. M. Ball, V. D'Innocenzo, C. Tao, S. Pathak, H. J. Snaith, A. Petrozza, F. De Angelis, *Energy Environ. Sci.* **2016**, 9, 155.
- [28] A. Al-Ashouri, A. Magomedov, M. Roß, M. Jošt, M. Talaikis, G. Chistiakova, T. Bertram, J. A. Márquez, E. Köhnen, E. Kasparavičius, S. Levenco, L. Gil-Escrig, C. J. Hages, R. Schlattmann, B. Rech, T. Malinauskas, T. Unold, C. A. Kaufmann, L. Korte, G. Niaura, V. Getautis, S. Albrecht, *Energy Environ. Sci.* **2019**, 12, 3356.
- [29] A. Czudek, K. Hirselandt, L. Kegelmann, A. Al-Ashouri, M. Jošt, W. Zuo, A. Abate, L. Korte, S. Albrecht, J. Dagar, E. L. Unger, arXiv:1906.05028, **2019**.
- [30] J. Dagar, K. Hirselandt, A. Merdasa, A. Czudek, R. Munir, F. Zu, N. Koch, T. Dittrich, E. L. Unger, *Sol. RRL* **2019**, 3, 1900088.
- [31] C. Schultz, M. Fenske, J. Dagar, A. Zeiser, A. Bartelt, R. Schlattmann, E. Unger, B. Stegemann, *Sol. Energy* **2020**, 198, 410.